OncoTargets and Therapy

Dovepress
Taylor & Francis Group

Open Access Full Text Article

ORIGINAL RESEARCH

Tumor-Infiltrating Mast Cells Enhance Neoadjuvant Therapy Efficacy in ESCC via Modulation of the Desmoplastic Microenvironment

Xing Cui[1,*], Xiangmei Zhang[2,3,*], Qi Zhao[1], Xin Chen[1,3], Ming He[1,3], Meng Zhang[4], Ruiling Yang[5], Jidong Zhao[1,3], Junfeng Liu[1]

[1]Department of Thoracic Surgery, Fourth Hospital of Hebei Medical University, Shijiazhuang, 050011, People's Republic of China; [2]Cancer Institute of Hebei Province, Fourth Hospital of Hebei Medical University, Shijiazhuang, 050011, People's Republic of China; [3]Hebei Provincial Key Laboratory of Tumor Microenvironment and Drug Resistance, Hebei Medical University, Shijiazhuang, 050017, People's Republic of China; [4]Department of Clinical Lab, Affiliated Hospital of Hebei University, Baoding, 071000, People's Republic of China; [5]Department of Breast Surgery, Handan Central Hospital, Handan, Hebei, 056000, People's Republic of China

*These authors contributed equally to this work

Correspondence: Jidong Zhao; Junfeng Liu, Email ud1291@126.com; 18939111700@189.cn

Objective: Neoadjuvant therapy is essential for locally advanced esophageal squamous cell carcinoma (ESCC), but its efficacy requires improvement. This study investigated the role of tumor-infiltrating mast cells (MCs) in treatment response and prognosis.

Methods: An integrated approach was employed, combining single-cell RNA sequencing of paired specimens from one ESCC patient pre- and post-neoadjuvant therapy, immunofluorescence analysis of a retrospective cohort of 68 treatment-naïve ESCC surgical specimens, bioinformatics analysis of public datasets, and in vitro mast cell activation assays.

Results: Single-cell sequencing revealed a post-therapy increase in the proportion of MCs among immune cells (4% to 12%), alongside an enriched inflammatory gene profile. In the cohort of 68 patients, higher MC density was associated with smaller tumor diameter (Pearson r = −0.32, p=0.007) and significantly better overall survival (36 vs 23.5 months, p=0.038). No such correlations were found for macrophages or CD8+ T cells. Bioinformatic analysis linked MCs to extracellular matrix and vascular smooth muscle regulation. Critically, high MC density combined with low desmoplasia or fibrosis identified patients with the most favorable prognosis. Phenotypically, MCs were predominantly non-degranulated in situ. In vitro, LPS activation (a non-degranulating signal) significantly upregulated CCL19 and other chemokines in mast cells. Furthermore, LPS was detected in the tumor stroma of 47.1% (32/68) of patients but not in normal mucosa.

Conclusion: The findings demonstrate that tumor-infiltrating MCs are associated with enhanced efficacy of neoadjuvant therapy and improved survival in ESCC. The mechanism may involve LPS-induced, non-degranulatory MC activation that modulates the desmoplastic microenvironment. Targeting this axis presents a promising strategy for ESCC treatment.

Keywords: tumor-infiltrating mast cells, desmoplasia, neoadjuvant therapy, non-degranulation, efficacy

Introduction

Esophageal cancer is a common malignant tumor of the upper digestive tract. Esophageal squamous cell carcinoma (ESCC) is the predominant histologic type in East Asia and ranks as the eighth most common malignancy globally. According to the latest epidemiological data, ESCC possesses the sixth highest mortality rate among all cancers, posing a severe threat to human health.[1] Current treatment primarily relies on surgery, with chemotherapy, radiotherapy, and immunotherapy serving as important adjuvant modalities. However, the clinical efficacy of these treatments is often limited by drug resistance, low sensitivity, and toxic side effects.[2]

https://doi.org/10.2147/OTT.S564090
Received: 29 August 2025
Accepted: 9 December 2025
Published: 14 January 2026

The tumor microenvironment (TME) is a critical determinant of the efficacy of chemotherapy, radiotherapy, and immunotherapy for solid tumors. The TME comprises not only tumor cells but also cancer-associated fibroblasts, immune cells, vascular networks, extracellular matrix (ECM), and various cytokines, which collectively support tumor survival and progression.[3] During proliferation and invasion, cancer cells secrete degrading enzymes and other active components to remodel the surrounding ECM.[4] This interaction frequently triggers an excessive deposition of fibrous connective tissue, a process known as desmoplasia, which is closely associated with tumor progression, metastasis, and patient prognosis.[5,6]

The accumulation of stromal components increases interstitial pressure, reduces blood flow and vascular density, thereby impeding drug delivery and contributing to treatment resistance.[7,8] The prognostic impact of stromal fibrosis and desmoplasia varies across cancer types, being strongly negative in pancreatic cancer but remaining controversial in breast, nasopharyngeal, and colorectal cancers.[9,10] The relationship between desmoplasia and prognosis in ESCC, however, is less clearly defined, warranting further investigation.

Mast cells (MCs) are versatile immune cells residing in various tissues, including tumors. In the TME, MCs exhibit dual roles, capable of either promoting or inhibiting tumor growth depending on context.[11,12] They store and secrete a vast array of bioactive mediators, such as proteases (eg, tryptase), histamine, prostaglandins, chemokines, and cytokines. Through these mediators, MCs can influence angiogenesis, immune cell recruitment, and fibroblast activation.[13,14] Notably, MC-derived tryptase and TGF-β can activate fibroblasts and promote collagen deposition, thereby driving interstitial fibrosis and connective tissue hyperplasia.[15,16] This MC-mediated desmoplasia can, in turn, create a physical barrier that blocks the infiltration of anti-tumor drugs and lymphocytes, potentially facilitating tumor invasion and metastasis.[17] Consequently, targeting MC activation and their pro-fibrotic functions represents a potential therapeutic strategy for cancers characterized by a dense stroma.

Our team's preliminary work and other reports suggest that MCs can activate fibroblasts and regulate their proliferation in the TME. However, the specific role of MCs in modulating the desmoplastic microenvironment of ESCC, and how this modulation ultimately influences the efficacy of neoadjuvant therapy, remains poorly understood. We hypothesized that tumor-infiltrating MCs, by modulating desmoplasia, could affect drug delivery and immune infiltration, thereby impacting treatment outcomes. To test this, we analyzed the relationship between MC density, interstitial fibrosis, desmoplastic reaction, and patient prognosis in ESCC. Furthermore, we investigated the phenotype of these MCs and their functional impact on the microenvironment to elucidate the potential mechanism linking MC-driven desmoplasia modulation to neoadjuvant therapy efficacy.

Metarials and Methods

Patients and Specimens

The study was conducted in accordance with the Declaration of Helsinki and approved by the Ethics Committee of the Fourth Hospital of Hebei Medical University. For single-cell sequencing analysis, paired specimens (pre-treatment endoscopic biopsies and post-treatment surgical resection) were obtained from one ESCC patient who received neoadjuvant therapy (anti-angiogenic drugs combined with chemotherapy). For histopathological and immunofluorescence analyses, a retrospective cohort was utilized, comprising postoperative paraffin-embedded tumor tissues from 68 ESCC patients who underwent primary surgical resection at the Fourth Hospital of Hebei Medical University between January 2021 and December 2023. The sample size for this cohort was determined by the availability of cases meeting the inclusion criteria during the study period. Key inclusion criteria were: (1) histologically confirmed ESCC; (2) underwent curative-intent surgery without preoperative neoadjuvant therapy; (3) availability of complete clinical and follow-up data. Exclusion criteria included: (1) presence of distant metastases at diagnosis; (2) history of other malignancies; (3) insufficient tissue quality for analysis. Paired para-carcinoma normal tissues were also collected for comparison.

Single-Cell RNA Sequencing

Single-cell suspensions were prepared from fresh tissue specimens. Briefly, approximately 10,000 cells per sample were loaded to capture ~8,000 cells per sample using the Chromium Single Cell A Chip kit and libraries were constructed

using the Single Cell 5' Library and Gel Bead Kit (10x Genomics, Pleasanton, CA, USA, #1000006) according to the manufacturer's instructions. Following barcoded reverse transcription within Gel Beads-in-emulsion (GEMs), cDNA was amplified and quality-assessed using an Agilent 2100 Bioanalyzer. Sequencing libraries were constructed and sequenced on an Illumina Novaseq6000 platform with a paired-end 150 bp (PE150) strategy, aiming for a minimum depth of 100,000 reads per cell. Raw sequencing data (fastq files) were aligned to the hg38 human reference genome and quantified using CellRanger software (version 6.0.0). Subsequent data analysis was performed in R (version 4.1.0) using the Seurat package (v4.1.0). Low-quality cells were filtered out based on the following criteria: unique molecular identifier (UMI) counts < 8,000, mitochondrial gene content > 75%, or ribosomal gene content < 45%. Potential doublets were removed using DoubletFinder (version 2.0.3). Data normalization, identification of highly variable genes, and log-normalization were performed using Seurat's NormalizeData and FindVariableFeatures functions. To integrate data from different samples and mitigate batch effects, the IntegrateData function was applied. Principal component analysis (PCA) and uniform manifold approximation and projection (UMAP) were performed on the integrated dataset for dimensionality reduction and visualization.

Histological Staining and Evaluation of Tissue Fibrosis and Desmoplasia

Formalin-fixed, paraffin-embedded (FFPE) ESCC resection specimens were sectioned at 5μm thickness, deparaffinized in xylene, rehydrated through a graded ethanol series, and stained with Hematoxylin & Eosin (H&E). The degree of stromal fibrosis was evaluated on H&E-stained sections and graded semi-quantitatively into three levels, adapted from previously published criteria:[18] Grade 1 (mild, fibrosis area < one-third of the tumor stroma), Grade 2 (moderate, fibrosis area between one-third and two-thirds), and Grade 3 (severe, fibrosis area > two-thirds). Furthermore, the desmoplastic microenvironment was categorized into three types based on the nature of the fibrotic matrix, as described by Ueno et al:[18] immature type (presence of myxoid changes in the matrix, regardless of keloid collagen), intermediate type (presence of keloid collagen without myxoid changes), and mature type (absence of both keloid collagen and myxoid changes). All histological evaluations were performed independently and in a blinded manner by two surgeons and one pathologist. The final category for each case was determined by the consensus of at least two evaluators.

Immunofluorescence Staining

Tissue Immunofluorescence

For FFPE tissue sections, after deparaffinization, rehydration, and microwave-assisted antigen retrieval in citrate buffer (pH 6.0), endogenous peroxidase activity was quenched with 3% hydrogen peroxide for 15 minutes. After blocking with 5% BSA for 1 hour, sections were incubated with primary antibodies against Tryptase (Abcam, ab2378, 1:200), LPS (Sigma-Aldrich, L4391, 1:300), CCL19 (R&D Systems, MAB361, 1:200), or CXCL8 (Invitrogen, MA5-23758, 1:200) either at 37°C for 1 hour or at 4°C overnight. Subsequently, sections were incubated with appropriate secondary antibodies, including biotinylated goat F(ab')2 anti-mouse IgG (Southern Biotechnology, 1031–08, 1:500) followed by streptavidin Alexa 488 (Invitrogen, S11223, 1:1000), or Rhodamine Red-X donkey F(ab')2 anti-rabbit IgG (Jackson ImmunoResearch, 711–295-152, 1:500), or NL637 donkey anti-goat IgG (R&D Systems, NL007, 1:200) for 1 hour at room temperature. To reduce autofluorescence, sections were treated with 0.1% Sudan Black B (Fisher Scientific, BP108-25) in 70% ethanol for 30 minutes. Nuclei were counterstained with DAPI (Vector Laboratories, H-1200), and slides were mounted and imaged using an Olympus BX53 fluorescence microscope.

Cell Immunofluorescence

For the cultured HMC-1 mast cell line, cells were fixed with 3.7% formaldehyde for 15 minutes at room temperature, permeabilized with 0.2% Triton X-100 in PBS for 10 minutes, and blocked with 5% BSA. Cells were then incubated with primary antibodies against Tryptase (1:200), CCL19 (1:200), or CXCL8 (1:200) for 1 hour at room temperature, followed by incubation with Alexa Fluor 488-conjugated donkey anti-mouse IgG (Invitrogen, A-21202, 1:1000) or Cy3-conjugated donkey anti-rabbit IgG (Jackson ImmunoResearch, 711–165-152, 1:1000) for 1 hour. Nuclei were stained with DAPI, and images were acquired using an Olympus IX73 inverted fluorescence microscope.

Bioinformatics Analysis

Gene expression data (FPKM values) and clinical information for esophageal carcinoma (ESCA cohort) were downloaded from The Cancer Genome Atlas (TCGA) database (https://portal.gdc.cancer.gov). Patients were stratified into high and low expression groups based on the median expression levels of mast cell-related genes KIT and FCER1A. Differentially expressed genes (DEGs) between these groups were identified using the *t*-test implemented in R, with an adjusted p-value (FDR) < 0.25 considered significant. The common DEGs shared between the KIT and FCER1A comparisons were identified and visualized using a Venn diagram. Functional enrichment analysis for Kyoto Encyclopedia of Genes and Genomes (KEGG) pathways and Gene Ontology (GO) terms was performed on the common DEGs using the R package ClusterProfiler (v3.14.3), with a significance threshold of $p < 0.05$.

Cell Culture and Activation

The human mast cell line HMC-1 (obtained from the Shanghai Institute of Biochemistry and Cell Biology, China) was cultured in Iscove's Modified Dulbecco's Medium (IMDM, Gibco, 12440053) supplemented with 10% fetal calf serum (FCS, Gibco, 10091–148) and 1% penicillin-streptomycin (Sigma-Aldrich, P0781) at 37°C in a 5% CO2 humidified incubator. For in vitro activation, HMC-1 cells (1×10^6 cells/well in a 6-well plate) were treated with Lipopolysaccharide (LPS, Sigma-Aldrich, L4391) at indicated concentrations (0.1 μg/mL or 1 μg/mL) for 6 hours. Cells treated with PBS vehicle alone served as the control. After treatment, cell pellets were collected for immunofluorescence staining, and culture supernatants were centrifuged at 3000 rpm for 10 min, aliquoted and stored at −80°C for subsequent analysis.

RNA Extraction and Quantitative Real-Time PCR (qRT-PCR)

Total RNA was extracted from HMC-1 cells using TRIzol reagent (Invitrogen, 15596026) according to the manufacturer's protocol. RNA concentration and purity were measured using a NanoDrop spectrophotometer. One microgram of total RNA was reverse-transcribed into cDNA using the TUREscript RT Master Mix reverse transcription kit (Aidlab, AT341). qRT-PCR was performed using the GO Taq qPCR Master Mix (Promega, A6002) on a QuantStudio 5 Real-Time PCR System (Applied Biosystems). The primer sequences (Sangon Biotech, Shanghai) used were:

Human TPSB2 (F: 5'-GACCACCACCACCAATTCCAAG-3'; R: 5'-TTAGTTGTTGTGTTGATTCTCAGTGTG-3'), Human CXCL8 (F: 5'-CCCATTCTTCTAAACAGCAGCATTC-3'; R: 5'-TGATTGAGAGGAGCCATCCAGATAG-3'), Human CCL19 (F: 5'-GTGGACCTGACCTGCCGTCTAG-3'; R: 5'-GAGTGGGTGTCGCTGTTGAAGTC-3'), Human GAPDH (F: 5'-GGAGCGAGATCCCTCCAAAAT-3'; R: 5'-GGCTGTTGTCATACTTCTCATGG-3').The cycling conditions consisted of 95°C for 10 minutes, followed by 40 cycles of 95°C for 15 seconds, 58°C for 30 seconds, and 72°C for 30 seconds. The relative expression levels of the target genes were calculated using the 2-ΔΔCT method with GAPDH as the endogenous control.

Statistical Analysis

SPSS 19.0 software (IBM Corporation) and GraphPad Prism 5 software (GraphPad Software, Inc.) were used for statistical and graphical analysis. Data from at least three independent experiments are presented as mean ± SEM. Differences between two groups were analyzed by Student's *t*-test, while comparisons among multiple groups were performed using one-way ANOVA followed by Tukey's post-hoc test. Survival analysis was conducted using the Kaplan-Meier method, and differences in survival curves were assessed by the Log rank test. A p-value of less than 0.05 was considered statistically significant.

Results

Elevated Proportion of Tumor-Infiltrating Mast Cells Following Effective Neoadjuvant Therapy

A representative case of advanced ESCC (grade III, stage III) received neoadjuvant therapy combining anti-angiogenic agents with a TC (taxane and platinum) regimen. After 4 cycles, significant tumor regression was observed (Figure 1A). Therapeutic efficacy was assessed by computed tomography (CT) scanning (Figure 1B) and histopathological examination of

H&E-stained sections (Figure 1C). We performed single-cell RNA sequencing on fresh tumor specimens obtained from this patient before and after neoadjuvant therapy. Analysis of the immune cell landscape revealed a notable shift: the proportion of mast cells among all immune cells increased from 4% pre-treatment to 12% post-treatment, even though the absolute number of mast cells decreased from 462 to 340 (Figure 1D and E). Gene expression profiling indicated that mast cells post-treatment exhibited enhanced expression of various cytokines (eg, IL1B, IL18, TNF) and chemokines (eg, CCL3, CCL4, CCL2, CXCL2, CXCL8) (Figure 1F). Concurrently, an increase in fibroblast numbers and the over-expression of multiple functional genes in fibroblasts were observed after treatment (Figure 1F).

High Density of Tumor-Infiltrating Mast Cells Correlates with Reduced Tumor Burden and Improved Survival

To characterize mast cell distribution in ESCC, we analyzed paired tumor and adjacent normal tissues from 68 treatment-naïve patients. Patient baseline characteristics are summarized in Table 1. H&E staining was used for general histology (Figure 2A–C), and immunofluorescence for tryptase was employed to identify mast cells (Figure 2B–D). Mast cells were predominantly located in the tumor stroma surrounding cancer nests. Comparative analysis revealed that 54 patients had lower mast cell density in tumor tissue compared to their normal mucosa (MC-low), while 14 patients had higher tumor mast cell density (MC-high) (Figure 2E). We observed a significant negative correlation between tumor-infiltrating mast cell density and both maximum tumor diameter (Pearson $r = -0.32$, $p = 0.007$) (Figure 2F) and pathological T stage (Pearson $r = -0.20$, $p = 0.09$) (Figure 2G). No significant correlations were found with tumor differentiation or lymph node metastasis (data not shown). Critically, patients in the MC-high group had significantly longer overall survival (36 ± 15.01 months) than those in the MC-low group (23.5 ± 17.07 months; Log rank test, $p = 0.038$) (Figure 2H).

For comparison, we also evaluated tumor-infiltrating macrophages (CD68+) and CD8+ T cells (Figure 3A). While both cell types were present at significantly higher densities in tumors compared to normal tissue (Figure 3B and C), their densities showed no significant correlation with tumor diameter (Figure 3D and E) or overall survival (Figure 3F and G).

Combined Analysis of Mast Cells and Desmoplasia Refines Prognostic Stratification

To explore the functional role of mast cells, we analyzed data from the TCGA-ESCC cohort. Expression of mast cell marker genes KIT and FCER1A was significantly lower in tumor tissues compared to normal esophageal samples (Figure 4A and B). Cross-analysis of differentially expressed genes between KIT/FCER1A high- and low-expression groups identified 87 shared genes (Figure 4C). Functional enrichment analysis (KEGG and GO) revealed that these mast cell-associated genes were primarily involved in "extracellular region" and "vascular smooth muscle contraction" (Figure 4D and E).

We next evaluated the desmoplastic microenvironment. Based on H&E staining, desmoplastic reaction was categorized as mature (mild, n=22) or immature (severe, n=46) (Figure 5A and B). While desmoplasia grade alone did not significantly stratify survival (Figure 5C), within the mature/mild desmoplasia subgroup, patients with high mast cell density (MC-high) had significantly better overall survival than those with low density (MC-low) (34.5 ± 19.14 vs 27.0 ± 16.56 months; $p = 0.037$) (Figure 5D). Similarly, stromal fibrosis was graded as mild (n=28) or severe (n=40) (Figure 5E and F). Fibrosis grade alone also did not impact survival (Figure 5G). However, within the mild fibrosis subgroup, MC-high patients again showed a significant survival advantage over MC-low patients (36.5 ± 21.99 vs 26.0 ± 12.76 months; $p = 0.027$) (Figure 5H).

LPS-Induced Non-Degranulatory Activation of Mast Cells Upregulates CCL19

We investigated the activation state of tumor-infiltrating mast cells. Immunofluorescence for tryptase showed that the majority of mast cells in both tumor and normal tissues retained tryptase within their cytoplasm, indicative of a non-degranulated phenotype (Figure 6A–C).

To model non-degranulatory activation in vitro, the human mast cell line HMC-1 was stimulated with LPS. This led to a dose-dependent upregulation of chemokine genes CCL19, CCL21, and CXCL8 (Figure 7A). Increased secretion of CCL19 and CXCL8 proteins was confirmed by immunofluorescence (Figure 7B and C). To support the potential relevance of this pathway in vivo, we detected LPS by immunofluorescence in the tumor stroma of 32 out of 68

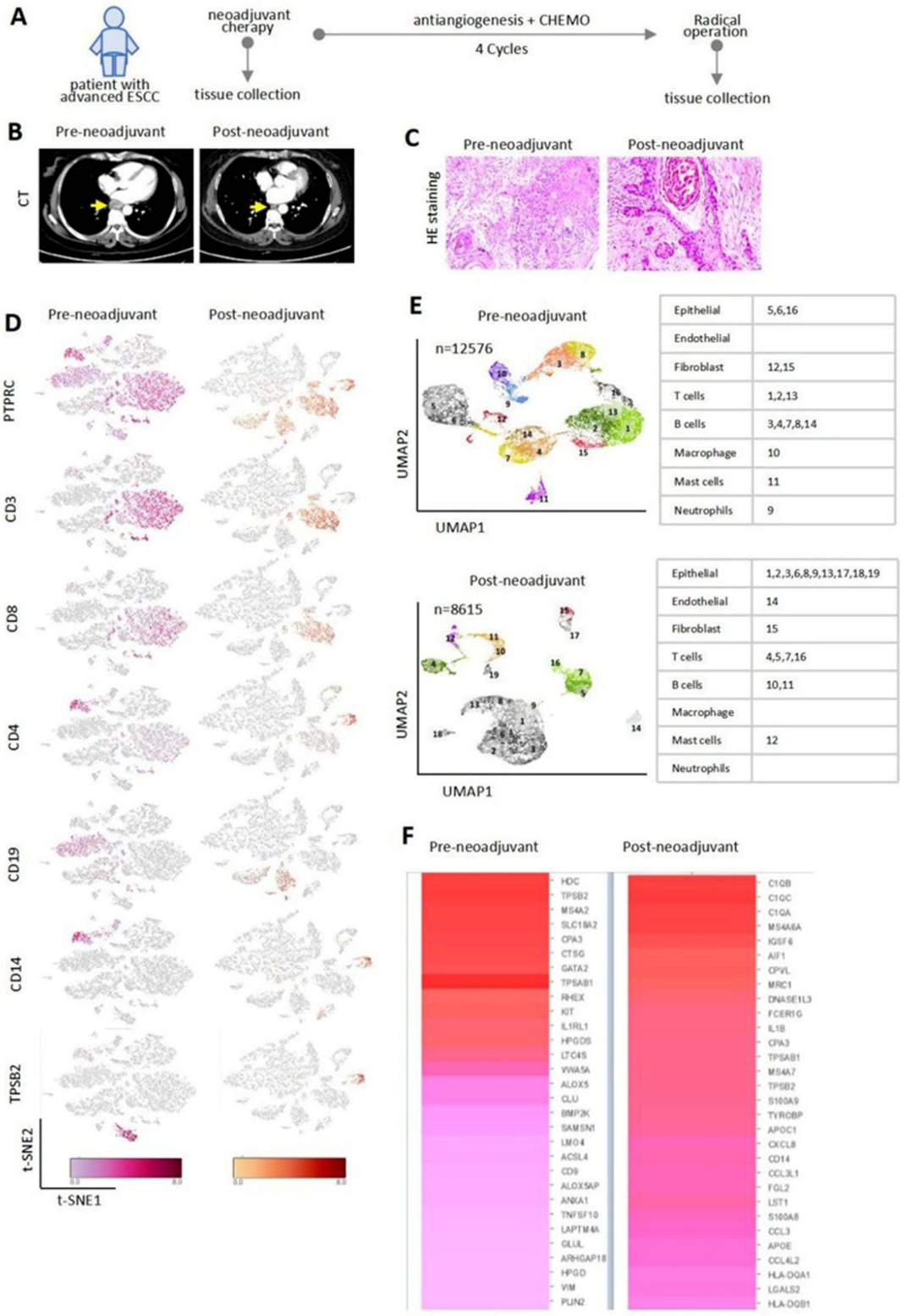

Figure 1 Elevated proportion of tumor-infiltrating mast cells after effective neoadjuvant therapy. (**A**) Scheme of treatment and specimen collection timeline. Therapeutic evaluation by (**B**) CT scanning and (**C**) H&E staining (scale bars, 100 μm). Single-cell sequencing analysis showing (**D** and **E**) the proportions of immune cell subsets and (**F**) a heatmap of the top 30 differentially expressed genes in mast cells and fibroblasts pre- and post-treatment.

https://doi.org/10.2147/OTT.S564090

Table 1 Baseline Characteristics of Patients with ESCC

Characteristics	Total Patients (n=68)	%
Age (years)		
Mean±SD	60±7.77	
Range	47~73	
Gender (n)		
Male	52	76.47
Female	16	23.53
Tumor location (n)		
Upper	16	23.53
Middle	42	61.76
Lower	10	14.71
Tumor differentiation (n)		
High	20	29.42
Middle	24	35.29
Low	24	35.29
Tumor size (cm)		
Mean±SD	4±1.65	
Range	1~9	
T stage (n)		
2	36	52.94
3	28	41.18
4	4	5.88
N stage (n)		
0	34	50.00
1	26	38.24
2	6	8.82
3	2	2.94

(47.1%) patients, with a distribution pattern similar to mast cells. In contrast, LPS was undetectable in normal esophageal mucosa (Figure 7D and E).

Discussions

The role of mast cells (MCs) in cancer has evolved beyond their classical function in allergy, emerging as a complex and context-dependent modulator of the tumor microenvironment (TME).[19,20] Our study provides clinical and mechanistic evidence in ESCC, demonstrating that a higher density of tumor-infiltrating MCs is associated with improved efficacy of neoadjuvant therapy and better patient survival. This protective association appears to be linked to a modulation of the desmoplastic microenvironment.[21]

A key and novel finding of our study is the observed increase in the relative proportion of MCs within the immune landscape following effective neoadjuvant therapy, as revealed by single-cell sequencing. This shift occurred alongside an enrichment of a pro-inflammatory gene signature in these MCs, suggesting a potential functional reprogramming rather than a passive accumulation. Furthermore, in our larger cohort, high MC density was correlated with smaller tumor size and superior overall survival, a relationship not observed for other immune cells like CD8+ T cells or macrophages. This underscores the unique and potentially pivotal role of MCs in ESCC progression and treatment response.

The function of MCs in cancer is notoriously pleiotropic, with studies reporting both pro-tumoral and anti-tumoral effects depending on the cancer type and context.[22,23] In certain malignancies, MCs are known to promote angiogenesis and immunosuppression.[24,25] However, our data in ESCC align with a growing body of evidence suggesting a protective role in some solid tumors.[26] The discrepancy may be explained by their activation state and subsequent mediator release

https://doi.org/10.2147/OTT.S564090

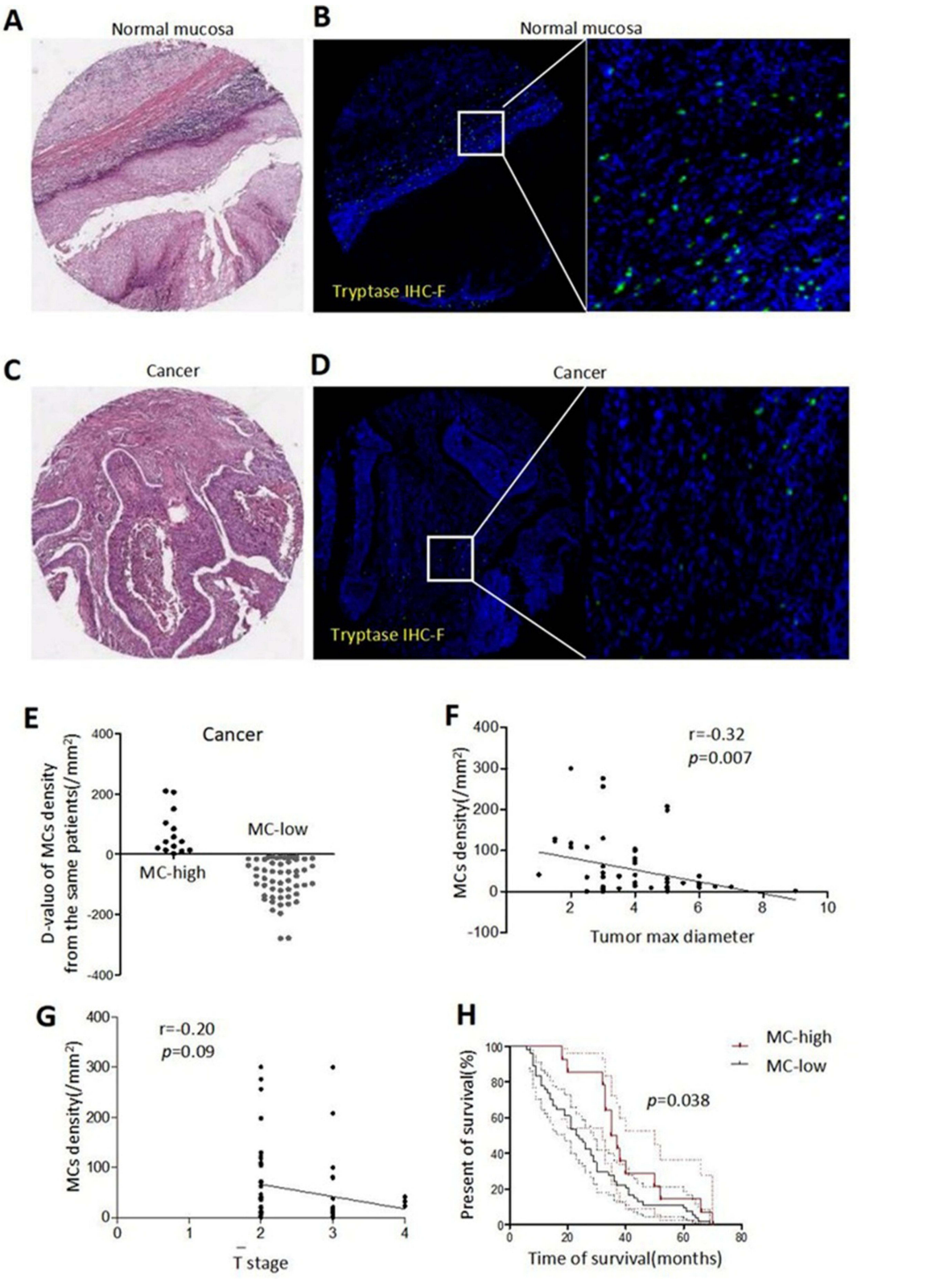

Figure 2 High density of tumor-infiltrating mast cells correlates with reduced tumor burden and improved survival. Representative H&E (**A**–**C**) and tryptase immunofluorescence (**B**–**D**) staining of normal mucosa and cancer tissue (scale bars, 100 μm; insets, 25 μm). (**E**) Classification of patients into MC-low and MC-high groups based on intra-tumoral mast cell density relative to paired normal tissue. Correlations between mast cell density and (**F**) tumor diameter and (**G**) pT stage. (**H**) Kaplan-Meier overall survival curves for MC-high and MC-low groups.

https://doi.org/10.2147/OTT.S564090

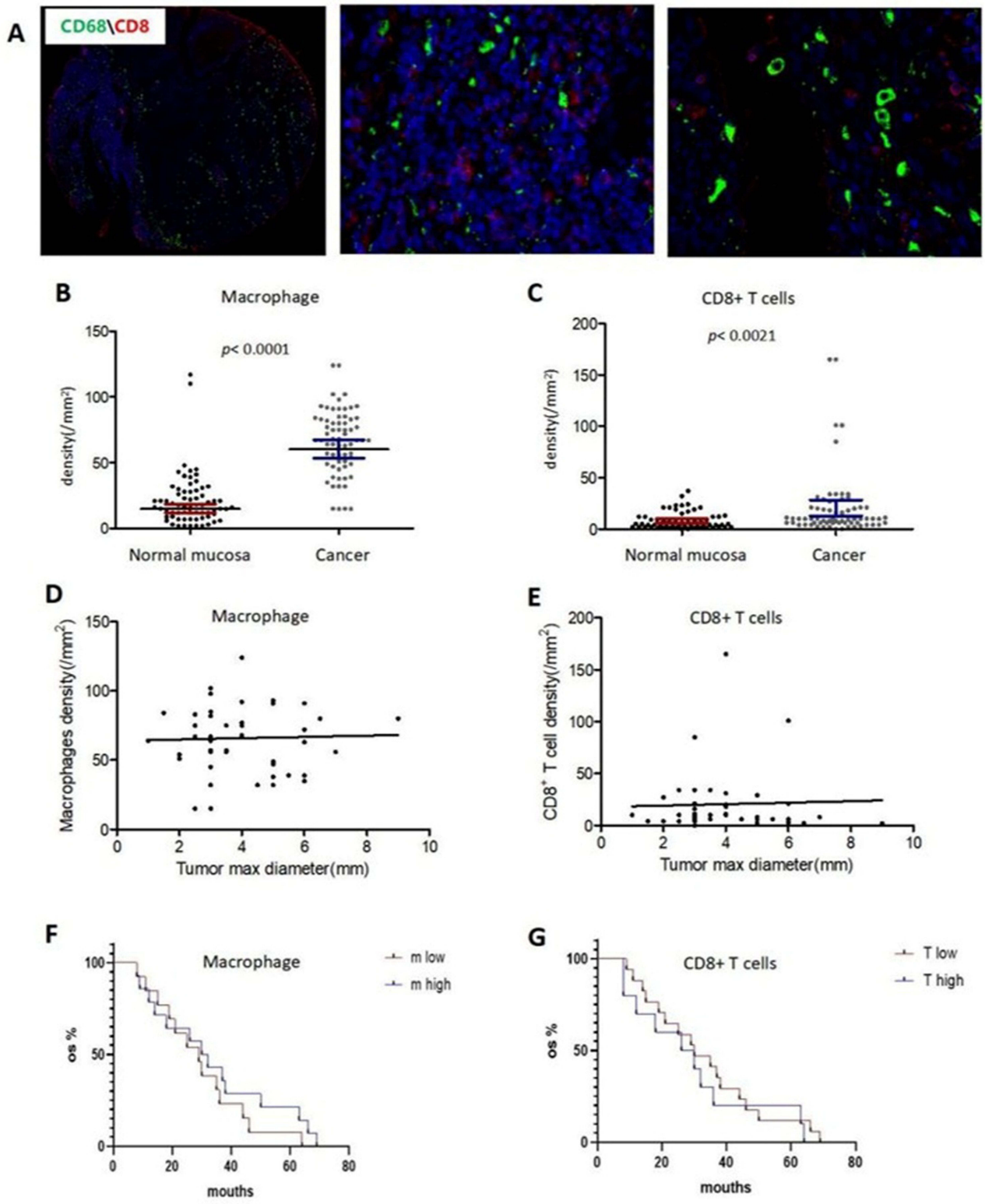

Figure 3 Analysis of tumor-infiltrating macrophages and CD8+ T cells. (**A**) Representative immunofluorescence images for CD68 (macrophages) and CD8 (T cells) (scale bars, 100 μm). Densities of (**B**) macrophages and (**C**) CD8+ T cells in tumor vs normal tissue. Correlations of cell density with (**D** and **E**) tumor diameter and (**F** and **G**) overall survival. *p < 0.05, **p < 0.01, **p < 0.001; ns, not significant.

https://doi.org/10.2147/OTT.S564090

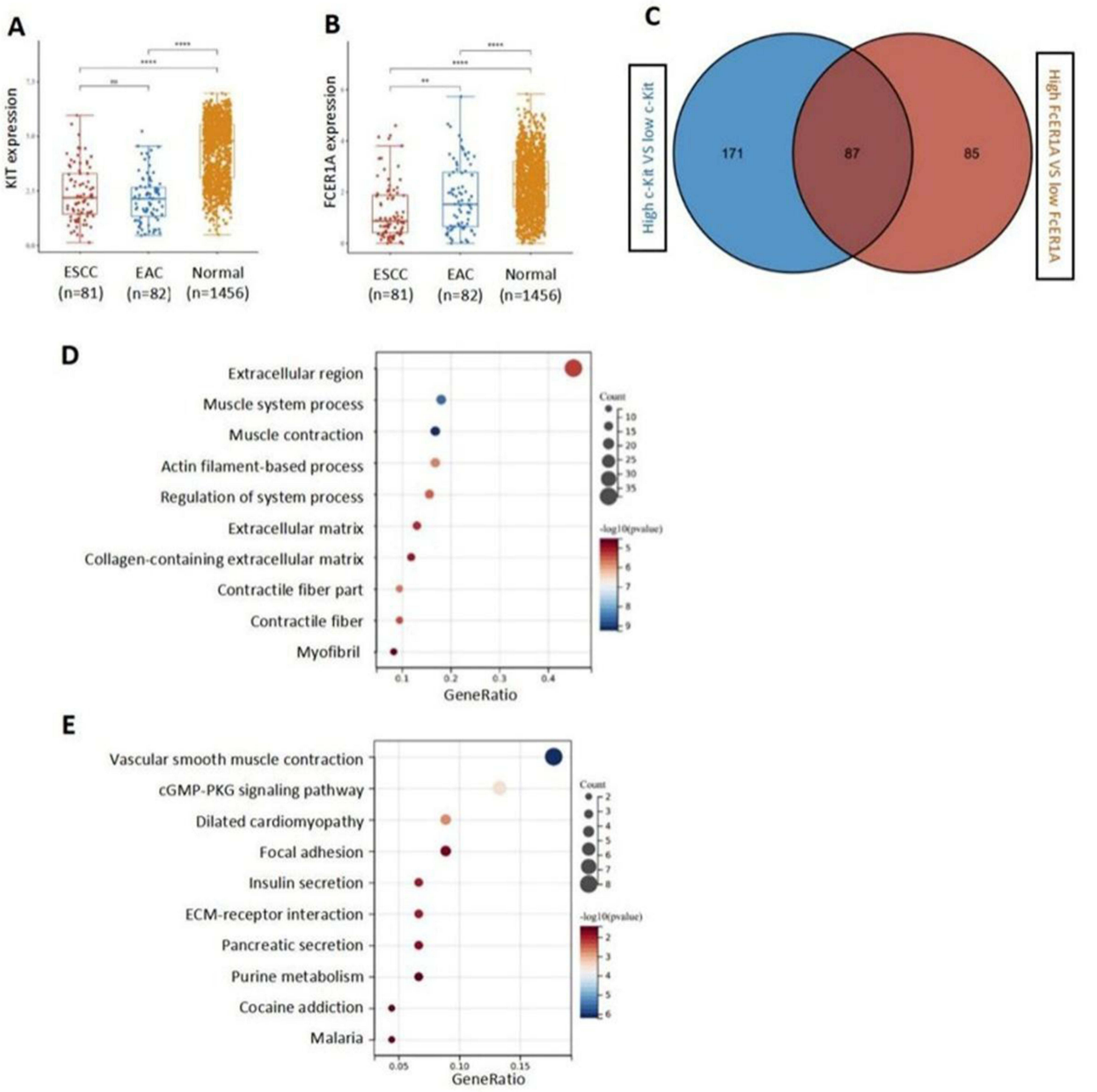

Figure 4 Bioinformatics analysis of mast cell-associated genes in ESCC. Expression of mast cell markers (**A**) KIT and (**B**) FCER1A in TCGA-ESCC data (***p < 0.01, ****p < 0.0001, *t*-test). (**C**) Venn diagram of overlapping DEGs. (**D**) GO term and (**E**) KEGG pathway enrichment analyses for the 87 shared genes.

profile.We identified that the majority of MCs in ESCC tissues were in a non-degranulated state, retaining mediators like tryptase intracellularly. This phenotype is consistent with activation via Toll-like receptors (TLRs), such as TLR4 by bacterial lipopolysaccharide (LPS), which can trigger sustained cytokine/chemokine secretion without massive, immediate degranulation.[13,15,16] Our bioinformatics analysis linked MCs in ESCC to processes like "vascular smooth muscle contraction," hinting at a potential role in regulating vessel tone and perfusion, which could influence drug delivery.

Crucially, we propose a mechanistic link between MCs and the desmoplastic stroma. Our in vitro experiments demonstrated that LPS activation of MCs robustly upregulated chemokines, particularly CCL19. CCL19 is a key chemokine involved in lymphocyte homing and has been implicated in extracellular matrix remodeling.[27,28] Therefore, we hypothesize that in the ESCC TME, MCs recruited and potentially activated by intratumoral bacteria (as suggested by our detection of LPS

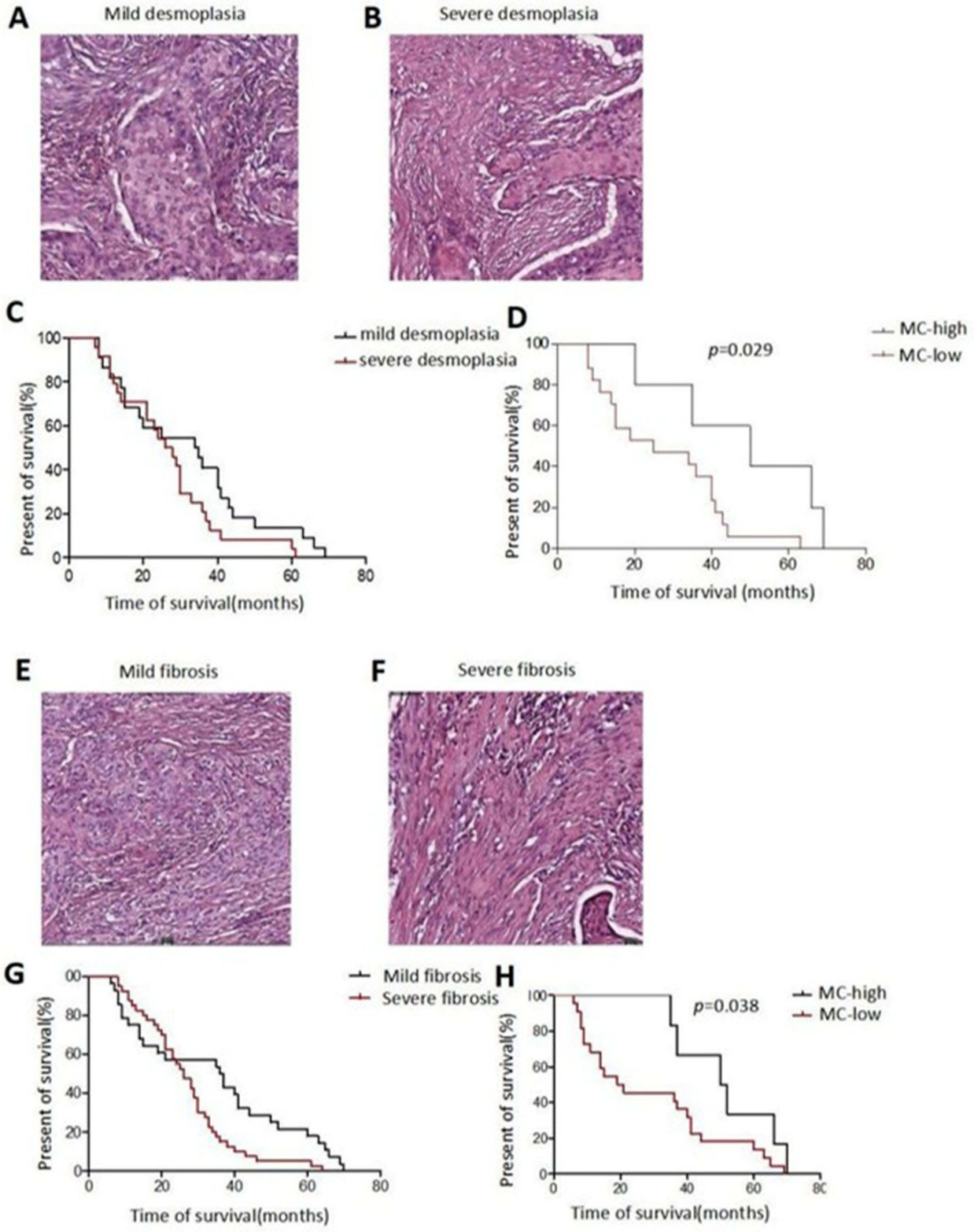

Figure 5 Prognostic value of combining mast cell density with desmoplasia and fibrosis assessment. Representative H&E images of (**A**) mature/mild and (**B**) immature/severe desmoplasia (scale bars, 100 μm). (**C** and **D**) Survival analysis by desmoplasia grade alone and combined with mast cell density. Representative H&E images of (**E**) mild and (**F**) severe fibrosis (scale bars, 100 μm). (**G** and **H**) Survival analysis by fibrosis grade alone and combined with mast cell density.

https://doi.org/10.2147/OTT.S564090

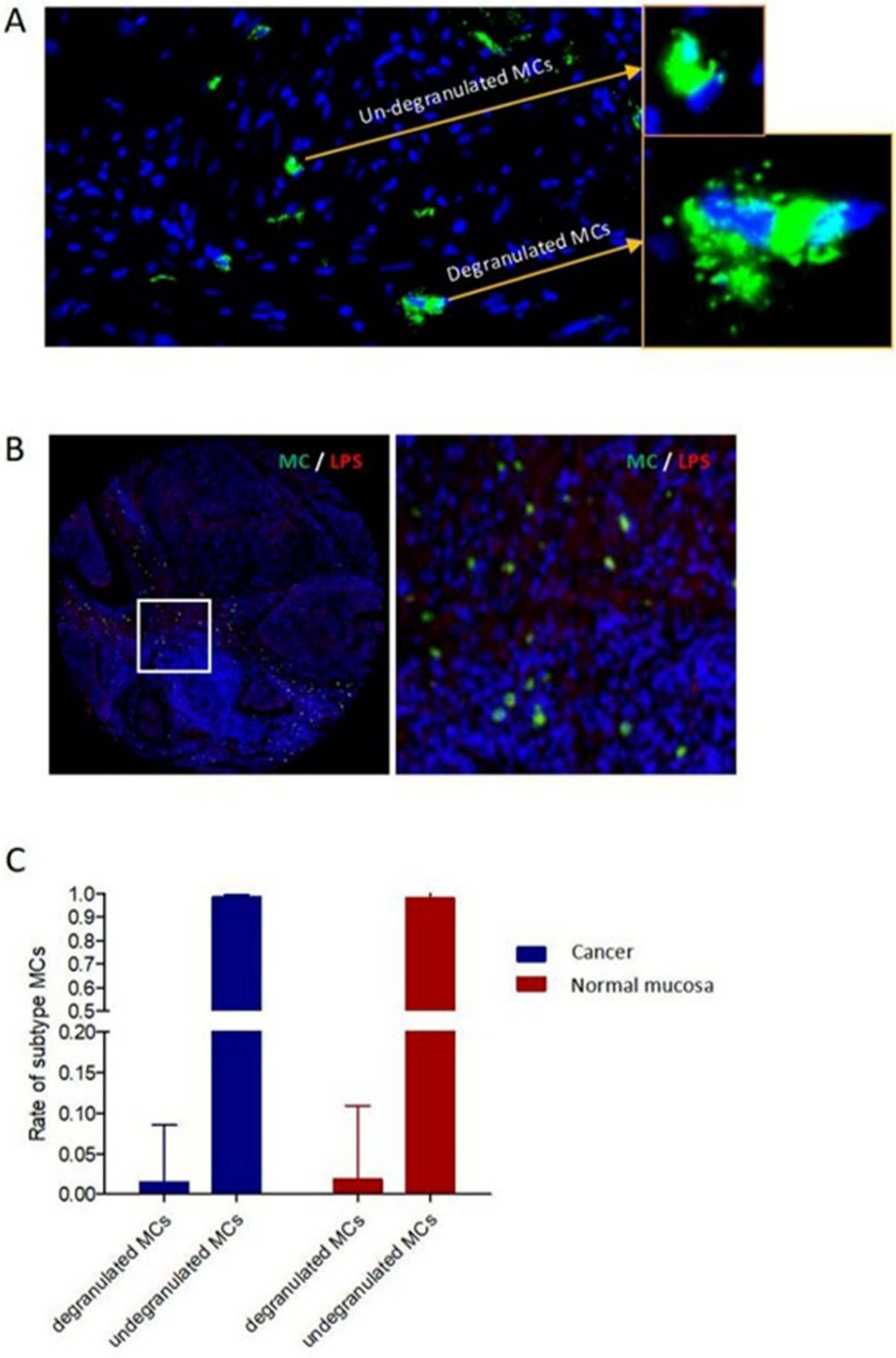

Figure 6 Mast cells in ESCC predominantly exhibit a non-degranulated phenotype. (**A** and **B**) Schematic and representative images illustrating degranulated vs non-degranulated mast cells based on tryptase distribution (scale bars, 25 μm). (**C**) Quantification of degranulation status in tumor and normal tissues.

in nearly half of the tumors) may secrete a spectrum of factors that help to maintain a less fibrotic, more organized stromal architecture.[29] This is supported by our clinical observation that the survival advantage of high MC density was most pronounced in patients with low-grade desmoplasia and fibrosis. A less dense, more mature stroma may facilitate enhanced perfusion and improved penetration of chemotherapeutic agents, thereby explaining the association with better neoadjuvant therapy efficacy.[7,8,17] This model reconciles our findings, positioning MCs as regulators of stromal composition whose activity can indirectly enhance treatment response.

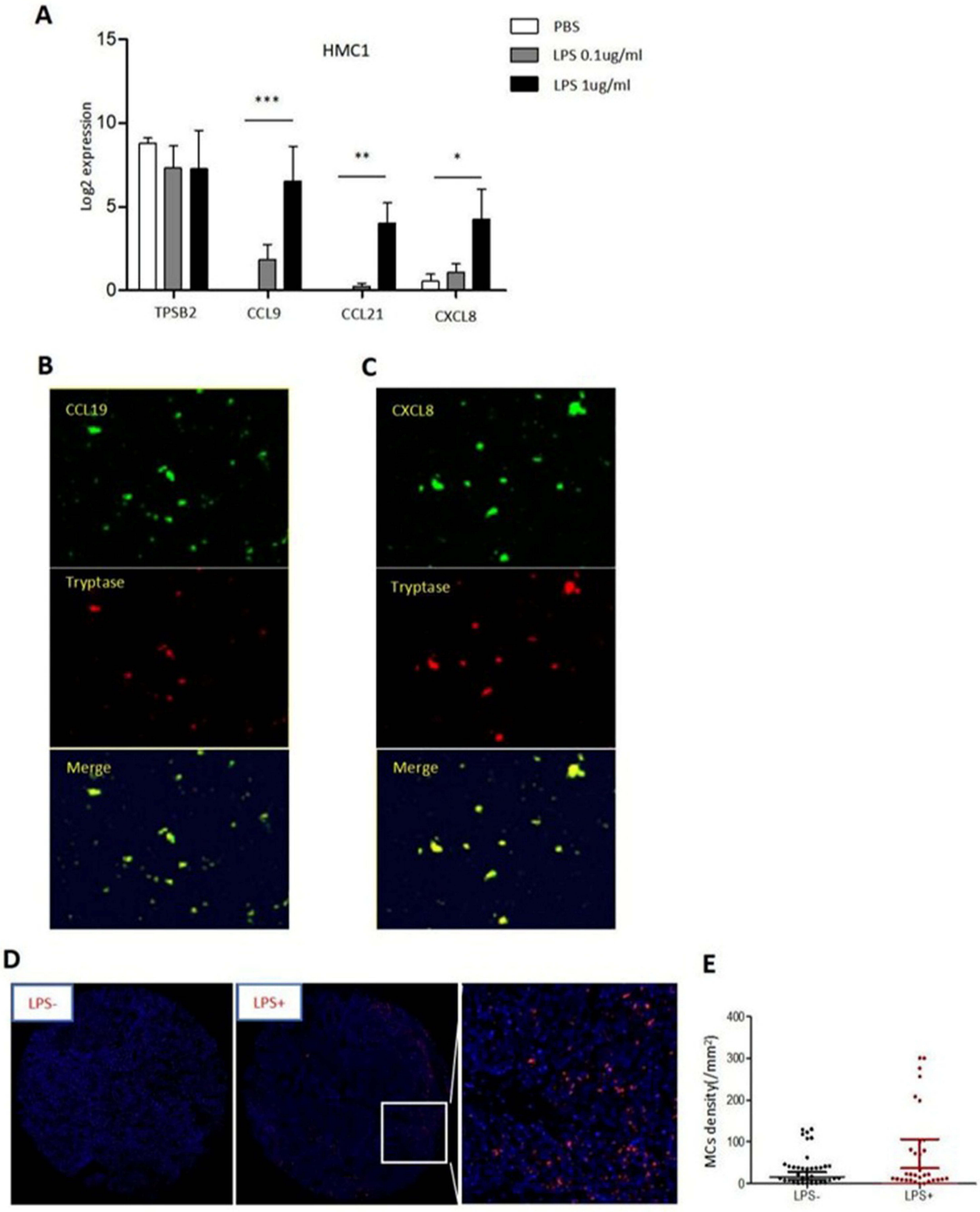

Figure 7 LPS induces chemokine production in mast cells and is present in the ESCC microenvironment. (**A**) qRT-PCR analysis of chemokine mRNA expression in HMC-1 cells after LPS stimulation. Immunofluorescence detection of (**B**) CCL19 and (**C**) CXCL8 in LPS-stimulated HMC-1 cells (scale bars, 25 μm). (**D**) Representative immunofluorescence images showing LPS expression in tumor tissue but not in normal mucosa (scale bars, 100 μm). (**E**) Quantification of LPS-positive patients. *p < 0.05, **p < 0.01, **p < 0.001.

https://doi.org/10.2147/OTT.S564090

Several limitations of our study should be acknowledged. Firstly, the retrospective nature of the cohort analysis and its single-center design necessitate validation in prospective, multi-center studies. Secondly, while our in vitro data support a functional role for LPS-activated MCs, the precise molecular mechanisms by which MC-derived factors directly modulate fibroblast activity and collagen deposition in the ESCC TME require further investigation, ideally through in vivo models. Finally, the specific source of intratumoral LPS and the full spectrum of MC-activating signals in ESCC remain to be fully elucidated.

Despite these limitations, our findings illuminate a promising therapeutic avenue. Future research should explore whether pharmacological modulation of MCs—for instance, by promoting their "favorable," non-degranulating phenotype or leveraging their chemokine secretion—can be harnessed to normalize the desmoplastic stroma. Such a strategy could be used as an adjuvant to enhance the efficacy of conventional neoadjuvant therapies in ESCC patients.

Conclusions

In conclusion, our integrated analysis suggests that tumor-infiltrating mast cells are associated with enhanced efficacy of neoadjuvant therapy and improved survival in ESCC. We propose that this effect is mediated, at least in part, through the modulation of the desmoplastic microenvironment. Mast cells, potentially activated by bacterial products like LPS in a non-degranulatory manner, may contribute to a stromal phenotype that is more permissive to drug delivery and anti-tumor activity. Therefore, targeting the crosstalk between mast cells and stromal components represents a potential novel strategy to improve therapeutic outcomes and patient prognosis in ESCC.

Ethics Approval

The study was conducted in accordance with the Declaration of Helsinki (2013 revision) and was approved by the Ethics Committee of the Fourth Hospital of Hebei Medical University (Approval No: 2017016). Informed consent was obtained from all patients.

Acknowledgment

The authors thank Dr. Xinhui Li and Dr. Tong Zhu for excellent technical assistance, and all the investigators for participating in this study.

Author Contributions

All authors made a significant contribution to the work reported, whether that is in the conception, study design, execution, acquisition of data, analysis and interpretation, or in all these areas; took part in drafting, revising or critically reviewing the article; gave final approval of the version to be published; have agreed on the journal to which the article has been submitted; and agree to be accountable for all aspects of the work.

Funding

This research are supported by Medical Science Research Project of Hebei No. 20180591 and Hebei Natural Science Foundation No. H2022206378.

Disclosure

The authors declare that they have no conflict of interest.

References

1. Brophy S, Cooksey R, Davies H, Dennis MS, Zhou SM, Siebert S. The effect of physical activity and motivation on function in ankylosing spondylitis: a cohort study. *Semin Arthritis Rheum*. 2013;42(6):619–626. doi:10.1016/j.semarthrit.2012.09.007
2. Vander Cruyssen B, Vastesaeger N, Collantes-Estévez E. Hip disease in ankylosing spondylitis. *Curr Opin Rheumatol*. 2013;25(4):448–454. doi:10.1097/BOR.0b013e3283620e04
3. Hamdi W, Chelli-Bouaziz M, Ahmed MS, et al. Correlations among clinical, radiographic, and sonographic scores for enthesitis in ankylosing spondylitis. *Joint Bone Spine*. 2011;78(3):270–274. doi:10.1016/j.jbspin.2010.09.010
4. Zhang HY, Liu R, Xing YJ, Xu P, Li Y, Li CJ. Effects of hypoxia on the proliferation, mineralization and ultrastructure of human periodontal ligament fibroblasts in vitro. *Exp Ther Med*. 2013;6(6):1553–1559. doi:10.3892/etm.2013.1349

5. Yang HS, Lu XH, Chen DY, et al. Upregulated expression of connexin43 in spinal ligament fibroblasts derived from patients presenting ossification of the posterior longitudinal ligament. *Spine*. 2011;36(26):2267–2274. doi:10.1097/BRS.0b013e31820ccfc6
6. Yamashita M, Iwama N, Date F, et al. Macrophages participate in lymphangiogenesis in idiopathic diffuse alveolar damage through CCL19-CCR7 signal. *Hum Pathol*. 2009;40(11):1553–1563. doi:10.1016/j.humpath.2009.03.021
7. Ziegler E, Oberbarnscheidt M, Bulfone-Paus S, Förster R, Kunzendorf U, Krautwald S. CCR7 signaling inhibits T cell proliferation. *J Immunol*. 2007;179(10):6485–6493. doi:10.4049/jimmunol.179.10.6485
8. Yang C, Deng X, Tang Y, Tang H, Xia C. Natural products reverse cisplatin resistance in the hypoxic tumor microenvironment. *Cancer Lett*. 2024;598:217116. doi:10.1016/j.canlet.2024.217116
9. Luther SA, Tang HL, Hyman PL, Farr AG, Cyster JG. Coexpression of the chemokines ELC and SLC by T zone stromal cells and deletion of the ELC gene in the plt/plt mouse. *Proc Natl Acad Sci U S A*. 2000;97(23):12694–12699. doi:10.1073/pnas.97.23.12694
10. Liu H, Tang L, Li Y, et al. Nasopharyngeal carcinoma: current views on the tumor microenvironment's impact on drug resistance and clinical outcomes. *Mol Cancer*. 2024;23(1):20. doi:10.1186/s12943-023-01928-2
11. Ribatti D. mast cells and resistance to immunotherapy in cancer. *Arch immunol ther exp*. 2023;71(1):11. doi:10.1007/s00005-023-00676-x
12. Longo V, Catino A, Montrone M, Galetta D, Ribatti D. Controversial role of mast cells in NSCLC tumor progression and angiogenesis. *Thoracic Cancer*. 2022;13(21):2929–2934. doi:10.1111/1759-7714.14654
13. Segura-Villalobos D, Ramírez-Moreno IG, Martínez-Aguilar M, et al. Mast cell-tumor interactions: molecular mechanisms of recruitment, intratumoral communication and potential therapeutic targets for tumor growth. *Cells*. 2022;11(3):349. doi:10.3390/cells11030349
14. Fergatova A, Affara NI. The cellular triumvirate: fibroblasts entangled in the crosstalk between cancer cells and immune cells. *FrontImmunol*. 2024;14:1337333. doi:10.3389/fimmu.2023.1337333
15. Savage A, Risquez C, Gomi K, et al. The mast cell exosome-fibroblast connection: a novel pro-fibrotic pathway. *Front Med*. 2023;10:1139397. doi:10.3389/fmed.2023.1139397
16. Wan J, Wu T, Liu Y, et al. Mast cells tryptase promotes intestinal fibrosis in natural decellularized intestinal scaffolds. *Tissue Eng and Regen Med*. 2022;19(4):717–726. doi:10.1007/s13770-022-00433-9
17. Panagi M, Mpekris F, Voutouri C, et al. Stabilizing tumor-resident mast cells restores t-cell infiltration and sensitizes sarcomas to PD-L1 inhibition. *Clin Cancer Res*. 2024;30(11):2582–2597. doi:10.1158/1078-0432.CCR-24-0246
18. Ueno H, Noll E, Diemunsch P, et al. Histologic Categorization of desmoplastic reaction: its relevance to the colorectal cancer microenvironment and prognosis. *Ann Surg*. 2014;259(4):700–707. doi:10.1097/SLA.0b013e31828d4ab3
19. Papa V, Li Pomi F, Di Gioacchino M, Mangifesta R, Borgia F, Gangemi S. Mast cells and microbiome in health and disease. *Front Biosci*. 2025;30(3):26283. doi:10.31083/FBL26283
20. Sánchez-Sánchez N, Riol-Blanco L, Rodríguez-Fernández JL. The multiple personalities of the chemokine receptor CCR7 in dendritic cells. *J Immunol*. 2006;176(9):5153–5159. doi:10.4049/jimmunol.176.9.5153
21. Nakashima M, Suga N, Ikeda Y, Yoshikawa S and Matsuda S. Relevant MicroRNAs of MMPs and TIMPs with Certain Gut Microbiota Could Be Involved in the Invasiveness and Metastasis of Malignant Tumors. *Innov Discov*. 2024;1(2). doi:10 10.53964/id.2024010
22. Pickens SR, Chamberlain ND, Volin MV, Pope RM, Mandelin AM 2nd, Shahrara S. Characterization of CCL19 and CCL21 in rheumatoid arthritis. *Arthritis Rheum*. 2011;63(4):914–922. doi:10.1002/art.30232
23. Nureki S, Miyazaki E, Ishi T, et al. Elevated concentrations of CCR7 ligands in patients with eosinophilic pneumonia. *Allergy*. 2013;68(11):1387–1395. doi:10.1111/all.12243
24. Cassier PA, Treilleux I, Bachelot T, et al. Prognostic value of the expression of C-Chemokine Receptor 6 and 7 and their ligands in non-metastatic breast cancer. *BMC Cancer*. 2011;11:213. doi:10.1186/1471-2407-11-213
25. Kostova I. Survey of Recent Trends of IB-IVB Metals and Their Compounds in Cancer Treatment. *Innov Discov*. 1(2):14. doi:10.53964/id.2024014
26. Mathes AL, Christmann RB, Stifano G, et al. Global chemokine expression in systemic sclerosis (SSc): CCL19 expression correlates with vascular inflammation in SSc skin. *Ann Rheum Dis*. 2014;73(10):1864–1872. doi:10.1136/annrheumdis-2012-202814
27. Gu Q, Zhou S, Chen C, et al. CCL19: a novel prognostic chemokine modulates the tumor immune microenvironment and outcomes of cancers. *Aging*. 2023;15(21):12369–12387. doi:10.18632/aging.205184
28. McGovern KE, Nance JP, David CN, et al. SPARC coordinates extracellular matrix remodeling and efficient recruitment to and migration of antigen-specific T cells in the brain following infection. *Sci Rep*. 2021;11(1):4549. doi:10.1038/s41598-021-83952-0
29. Deep Kaur S and Kapoor ND. Role of Soy-derived Peptide Lunasin in Cancer Therapy: A Review. *Innov Discov*. 2025;2(4):17. doi:10.53964/id.2025017